J. Phys. B: At. Mol. Opt. Phys. **43** (2010) 065101 (13pp) doi:10.1088/0953-4075/43/6/065101

Ab initio calculation of the 66 low-lying electronic states of HeH^+: adiabatic and diabatic representations

Jérôme Loreau[1], Jacques Liévin[1], Patrick Palmeri[2], Pascal Quinet[2,3] and Nathalie Vaeck[1]

[1] Laboratoire de Chimie Quantique et Photophysique, Faculté des Sciences, Université Libre de Bruxelles, 50, av. F. Roosevelt, CP160/09, 1050 Bruxelles, Belgium
[2] Service d'Astrophysique et de Spectroscopie, Université de Mons, 20 Place du Parc, B-7000 Mons, Belgium
[3] IPNAS, Université de Liège, Bat.15, Sart Tilman, B-4000 Liège, Belgium

E-mail: nvaeck@ulb.ac.be

Received 23 November 2009, in final form 6 January 2010
Published 2 March 2010
Online at stacks.iop.org/JPhysB/43/065101

Abstract
Using the quantum chemistry package MOLPRO and an adapted basis set, we have calculated the adiabatic potential energy curves of the first 20 $^1\Sigma^+$, 19 $^3\Sigma^+$, 12 $^1\Pi$, 9 $^3\Pi$, 4 $^1\Delta$ and 2 $^3\Delta$ electronic states of the HeH^+ molecular ion in CASSCF and CI approaches. The results are compared with previous works. The radial and rotational non-adiabatic coupling matrix elements as well as the dipole moments are also calculated. The asymptotic behaviour of the potential energy curves and of the various couplings between the states is also studied. Using the radial couplings, the diabatic representation is defined and we present an example of our diabatization procedure on the $^1\Sigma^+$ states.

(Some figures in this article are in colour only in the electronic version)

1. Introduction

HeH^+, or hydrohelium cation, is thought to be the first molecular species to appear in the Universe, its formation being due to radiative association between H^+ and He (Roberge and Dalgarno 1982). In addition, the high fractional abundance of HeH^+ should allow its detection in stars formed from primordial material such as the recently discovered very metal-poor stars HE1327−2326 and HE0107−5240 (Frebel *et al* 2005) or in He-rich environment as in the white dwarfs SDSS J133739+000142 and LHS 3250 (Harris *et al* 2004). The inclusion of HeH^+ in the existing atmospherical models of those objects could have serious implications. It should also be present in the planetary nebula NGC7027 but has eluded observation (Moorhead *et al* 1988). In fact, up to now, none of the several attempts to extraterrestrial observation of HeH^+ have been conclusive (Engel *et al* 2005). Considering that the excited states of HeH^+ are too shallow or unstable to support a visible or UV spectrum, those assessments have risen up a number of studies to obtain theoretically and experimentally the most accurate rotational spectrum of HeH^+ in the ground state, culminating with the recent work of Stanke *et al* (2006). In addition to extremely accurate knowledge of the spectroscopic properties of the hydrohelium cation, the various mechanisms leading to its formation or decay must be investigated to obtain a correct estimation of the population of the levels. In this context, the first experimental data for the photodissociation cross section in the far UV have been obtained recently using the free electron laser FLASH at Hambourg (Pedersen *et al* 2007), showing important disagreement with the previous theoretical works and motivating new calculations (Sodoga *et al* 2009, Dumitriu and Saenz 2009).

Despite the fact that its astrophysical observation is still questionable, HeH^+ is clearly present in helium–hydrogen laboratory plasmas. Indeed, since its first observation in mass spectrometry of discharges in mixtures of helium and hydrogen in 1925 (Hogness and Lunn 1925), HeH^+ has been found to be one of the major components in other He/H plasma sources such as high-voltage glow discharges, synchrotron

devices, inductively coupled plasma generators, capacitively coupled RF discharges and magnetically confined plasmas, the last one playing of course a very special role in today's development of thermonuclear fusion. Helium emission lines have been proposed recently as a diagnostic tool for divertor regions of the tokamak. However, to model the intensity of these emission lines, knowledge of the cross sections of the charge transfer processes which populate the emitting levels of helium up to $n = 4$ is essential. At low or very low collisional energy, the theoretical description of charge transfer requires a molecular approach and the calculation of the excited states of the HeH^+ quasi-molecule (Rosmej *et al* 2006).

From a theoretical point of view, the hydrohelium cation is the simplest closed-shell heteronuclear molecule and therefore a considerable amount of work has been dedicated to high-precision calculations of its ground state, including accurate description of relativistic and non-adiabatic effects (Stanke *et al* 2008). In a lesser measure, the first excited states have also been used to assess the efficiency of different *ab initio* methods to describe states that are not the lowest of their symmetry (Richings and Karadakov 2007) or to understand and remedy the failure of time-dependent density functional theory to provide accurate charge transfer excitation energies (Giesbertz *et al* 2008). The most complete study of the excited states of HeH^+ has been performed by Green *et al* in a series of four articles (Green *et al* 1974a, 1974b, 1976, 1978). States up to $n = 3$ (where n is the highest principal quantum number in the dissociation configuration of hydrogen or helium) have been calculated using a CI (configuration interaction) method with a combination of Slater-type orbitals and ellipsoidal orbitals. Despite the fact that this exhaustive study includes the calculation of dipole matrix elements and radial non-adiabatic couplings, its accuracy has never been assessed and the use of these results directly in quantum molecular dynamics programs is problematic due to the lack of data for medium or large internuclear distances.

While the first excited states of the neutral HeH molecule emanate from the excitation of the hydrogen atom alone, the first part of the electronic spectrum of HeH^+ results from a mixing between states arising from single excitations of neutral helium or hydrogen. The higher part of the spectrum is built upon single excitations of the He^+ cation as well as double excitations of neutral helium and of the ground state of the H^- anion.

The purpose of this paper is to reexamine the first part of the electronic spectrum of a HeH^+ molecule and to extend its description up to $n = 4$ with high-level *ab initio* quantum chemistry methods in order to provide adequate material required for both spectroscopy and dynamical studies such as charge transfer processes in excited states (Loreau *et al* 2010) or photodissociation in the far UV domain (Sodoga *et al* 2009). In addition, the diabatic representation of the potential energy curves is investigated. The results of the present work are compared to the corresponding data in the literature, when available.

All the data described in this paper are accessible on demand to the corresponding author of this paper.

2. One electron basis set and asymptotic atomic energy levels

One problem encountered in this work is the construction of a reliable Gaussian basis set allowing the description of the formation of the HeH^+ molecular ion from the first Rydberg states of the H and He atoms up to $n = 4$. As mentioned above, the first part of the electronic spectrum corresponds indeed asymptotically to the excitation of both hydrogen and neutral helium. Therefore, our basis set consists for each atom of the aug-cc-pV5Z basis set (Dunning 1989, Woon and Dunning 1994) augmented by $[3s, 3p, 2d, 1f]$ Gaussian-type orbitals optimized to reproduce the spectroscopic orbitals of the He and H excited states. A different atomic basis has been developed up to $n = 4$ for He depending on whether the molecular state under consideration is a singlet or a triplet state. Those additional sets of orbitals have been obtained by fitting Slater-type orbitals from calculations performed for each atomic state using the AUTOSTRUCTURE package (Eissner *et al* 1974, Badnell 1986, 1997). In total, a $[8s, 7p, 5d, 3f, 1g]$ basis set has been used for both atoms. The additional orbitals and their contraction coefficients are given in the appendix.

For all values of ℓ, this basis set reproduces the exact non-relativistic atomic levels of hydrogen up to $n = 3$ within 15 cm^{-1}. The electronegativity of H^- deviates from the experimental value from 37 cm^{-1} in a full CI level of approximation. Different Gaussian basis sets have already been proposed in the literature mainly for the calculation of the ground state of HeH^+ (Jurek *et al* 1995 and references therein) or the ground and excited states of the neutral HeH molecule which correspond asymptotically to excitations of H up to $n = 3$ (van Hemert and Peyerimhoff 1990). Using this last atomic basis set, the levels for the hydrogen atom are reproduced within 20 cm^{-1} for the s and p states and within 70 cm^{-1} for the d state.

In the non-relativistic approximation, the $1s n\ell$ ($n = 1$–3) levels of helium are described at a full CI level by our basis set within 115 cm^{-1} for s states, 60 cm^{-1} for p states and 30 cm^{-1} for d states.

For both atoms, the s states for $n = 4$ are more difficult to reproduce, mainly due to the lack of upper states and the large number of lower states, but are still in a reasonable agreement (145 cm^{-1} at most) with the exact values. The other $n = 4$ states are reproduced within 42 cm^{-1} for both atoms.

In conclusion, although this basis set is rather small, it is adapted to the HeH^+ system and will allow a correct description of the potential energy curves as well as the determination of the non-adiabatic couplings which, in our approach, require CASSCF (complete active space self-consistent field) calculations.

3. Potential energy curves

The Born–Oppenheimer adiabatic potential energy curves (PEC) for the lowest molecular states corresponding asymptotically to excitation in the $n = 1$–4 atomic shells have been calculated as a function of the internuclear distance R using the MOLPRO molecular structure package

Table 1. $^1\Sigma^+$ states included in the calculations and their dissociation product. In this table, we use the notation H($n\ell$) or He($1sn\ell\,^1L$) to denote the electronic wavefunctions of the corresponding electronic states. Due to the He^+ charge, there is a Stark effect on the hydrogen levels (see the text). The mixing coefficients have been calculated by diagonalizing the perturbation matrix due to the electric field.

	m	Energy (hartree) at $R = 70$ au	Dissociative atomic wavefunctions[a]
$n = 1$	1	−2.903 243 07	He($1s^2$)
	2	−2.499 955 02	H($1s$)
$n = 2$	3	−2.145 894 24	He($1s2s\,^1S$)
	4	−2.125 564 99	$\frac{1}{\sqrt{2}}$ H($2s$) + $\frac{1}{\sqrt{2}}$ H($2p$)
	5	−2.124 337 65	$\frac{1}{\sqrt{2}}$H($2s$) − $\frac{1}{\sqrt{2}}$H($2p$)
	6	−2.123 740 55	He($1s2p\,^1P^o$)
$n = 3$	7	−2.061 570 66	He($1s3s\,^1S$)
	8	−2.057 583 00	$\frac{1}{\sqrt{3}}$H($3s$) − $\frac{1}{\sqrt{2}}$H($3p$) + $\frac{1}{\sqrt{6}}$H($3d$)
	9	−2.056 327 93	He($1s3d\,^1D$)
	10	−2.055 370 40	$\frac{1}{\sqrt{3}}$H($3s$) − $\sqrt{\frac{2}{3}}$H($3d$)
	11	−2.053 791 72	He($1s3p\,^1P^o$)
	12	−2.054 118 89	$\frac{1}{\sqrt{3}}$H($3s$) + $\frac{1}{\sqrt{2}}$H($3p$) + $\frac{1}{\sqrt{6}}$H($3d$)
$n = 4$	13	−2.037 018 79	He($1s4s\,^1S$)
	14	−2.035 020 13	$\frac{1}{2}$H($4s$) − $\frac{3}{2\sqrt{5}}$H($4p$) + $\frac{1}{2}$H($4d$) − $\frac{1}{2\sqrt{5}}$H($4f$)
	15	−2.032 668 13	He($1s4f\,^1F^o$)
	16	−2.031 948 05	$\frac{1}{2}$H($4s$) − $\frac{1}{2\sqrt{5}}$H($4p$) − $\frac{1}{2}$H($4d$) + $\frac{3}{2\sqrt{5}}$H($4f$)
	17	−2.030 279 98	He($1s4d\,^1D$)
	18	−2.029 618 68	$\frac{1}{2}$H($4s$) + $\frac{1}{2\sqrt{5}}$H($4p$) − $\frac{1}{2}$H($4d$) − $\frac{3}{2\sqrt{5}}$H($4f$)
	19	−2.028 511 59	He($1s4p\,^1P^o$)
	20	−2.028 023 90	$\frac{1}{2}$H($4s$) + $\frac{3}{2\sqrt{5}}$H($4p$) + $\frac{1}{2}$H($4d$) + $\frac{1}{2\sqrt{5}}$H($4f$)

[a] It is understood that H($n\ell$) is accompanied by $He^+(1s)$ and that He($1sn\ell\,^1L$) is accompanied by H^+.

Table 2. $^3\Sigma^+$ states states included in the calculations and their dissociation product. In this table, we use the notation H($n\ell$) or He($1sn\ell\,^3L$) to denote the electronic wavefunctions of the corresponding electronic states. Due to the He^+ charge, there is a Stark effect on the hydrogen levels (see the text). The mixing coefficients have been calculated by diagonalizing the perturbation matrix due to the electric field.

	m	Energy (hartree) at $R = 70$ au	Dissociative atomic wavefunctions[a]
$n = 1$	1	−2.499 960 40	H($1s$)
$n = 2$	2	−2.175 134 28	He($1s2s\,^3S$)
	3	−2.132 884 67	He($1s2p\,^3P^o$)
	4	−2.125 570 46	$\frac{1}{\sqrt{2}}$H($2s$) + $\frac{1}{\sqrt{2}}$H($2p$))
	5	−2.124 343 10	$\frac{1}{\sqrt{2}}$H($2s$) − $\frac{1}{\sqrt{2}}$H($2p$)
$n = 3$	6	−2.068 801 05	He($1s3s\,^3S$)
	7	−2.058 414 57	He($1s3p\,^3P^o$)
	8	−2.057 588 56	$\frac{1}{\sqrt{3}}$H($3s$) − $\frac{1}{\sqrt{2}}$H($3p$) + $\frac{1}{\sqrt{6}}$H($3d$)
	9	−2.055 375 99	$\frac{1}{\sqrt{3}}$H($3s$) − $\sqrt{\frac{2}{3}}$H($3d$)
	10	−2.055 206 40	He($1s3d\,^3D$)
	11	−2.053 797 35	$\frac{1}{\sqrt{3}}$H($3s$) + $\frac{1}{\sqrt{2}}$H($3p$) + $\frac{1}{\sqrt{6}}$H($3d$)
$n = 4$	12	−2.038 140 67	He($1s4s\,^3S$)
	13	−2.035 621 21	He($1s4p\,^3P^o$)
	14	−2.032 924 54	$\frac{1}{2}$H($4s$) − $\frac{3}{2\sqrt{5}}$H($4p$) + $\frac{1}{2}$H($4d$) − $\frac{1}{2\sqrt{5}}$H($4f$)
	15	−2.031 955 57	$\frac{1}{2}$H($4s$) − $\frac{1}{2\sqrt{5}}$H($4p$) − $\frac{1}{2}$H($4d$) + $\frac{3}{2\sqrt{5}}$H($4f$)
	16	−2.029 628 42	He($1s4d\,^3D$)
	17	−2.029 559 29	$\frac{1}{2}$H($4s$) + $\frac{1}{2\sqrt{5}}$H($4p$) − $\frac{1}{2}$H($4d$) − $\frac{3}{2\sqrt{5}}$H($4f$)
	18	−2.028 033 85	$\frac{3}{2\sqrt{5}}$H($4p$) + $\frac{1}{2}$H($4d$) + $\frac{1}{2\sqrt{5}}$H($4f$)
	19	−2.016 557 85	He($1s4f\,^3F^o$)

[a] It is understood that H($n\ell$) is accompanied by $He^+(1s)$ and that He($1sn\ell\,^3L$) is accompanied by H^+.

(Werner *et al* 2006). This includes 20 $^1\Sigma^+$, 19 $^3\Sigma^+$, 12 $^1\Pi$, 9 $^3\Pi$, 4 $^1\Delta$ and 2 $^3\Delta$ states, which constitute a total of 66 electronic states. All these states, as well as their energy at $R = 70$ au and their dissociation products, are presented in tables 1–6. To obtain the PEC, we performed a state-averaged CASSCF (Werner and Knowles 1985, Knowles and Werner 1985) using the active spaces listed in table 7, followed by a full CI.

As we will not consider any spin-dependent interaction, the singlet and triplet states can be calculated separately.

3.1. Adiabatic $n = 1$ potential energy curves

The $n = 1$ states consist of two $^1\Sigma^+$ and one $^3\Sigma^+$ states and are shown in figure 1. All three are bound states that support a vibrational structure.

Our calculations reproduce correctly the equilibrium distance of 1.463 au of the $X\,^1\Sigma^+$ state. The dissociation energy of the ground state calculated by Kolos and Peek (1976) is D_e = 16 455.64 cm^{-1} and a more accurate value of 16 456.51 cm^{-1}, which include diagonal Born–Oppenheimer corrections, was given by Bishop and Cheung (1979). From an experimental point of view, a numerical procedure particularly successful when data are fragmentary has been employed by Coxon and Hajigeorgiou (1999) to inverse the spectroscopic

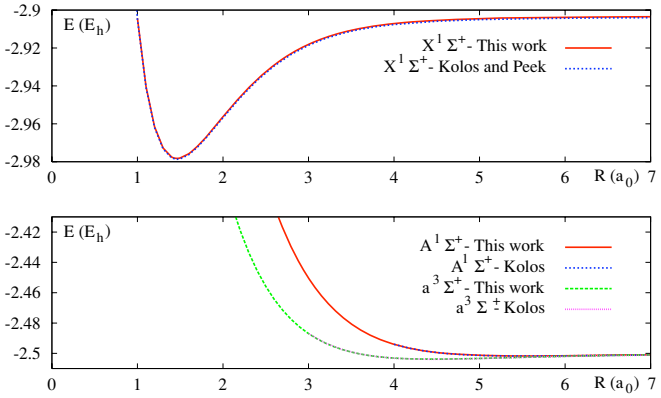

Figure 1. Adiabatic potential energy curves (in hartrees) of the $n = 1$ states. Comparison with the work of Kolos (1976) and Kolos and Peek (1976).

Table 3. $^1\Pi$ states included in the calculations and their dissociation product. In this table, we use the notation H($n\ell$) or He($1sn\ell\,^1L$) to denote the electronic wavefunctions of the corresponding electronic states. Due to the He^+ charge, there is a Stark effect on the hydrogen levels (see the text). The mixing coefficients have been calculated by diagonalizing the perturbation matrix due to the electric field.

	m	Energy (hartree) at $R = 70$ au	Dissociative atomic wavefunctions[a]
$n = 2$	1	−2.124 916 60	H($2p$)
	2	−2.123 684 73	He($1s2p\,^1P^o$)
$n = 3$	3	−2.056 398 37	$\frac{1}{\sqrt{2}}$H($3p$) + $\frac{1}{\sqrt{2}}$H($3d$)
	4	−2.056 164 25	He($1s3d\,^1D$)
	5	−2.054 563 33	$\frac{1}{\sqrt{2}}$H($3p$) − $\frac{1}{\sqrt{2}}$H($3d$)
	6	−2.054 198 37	He($1s3p\,^1P^o$)
$n = 4$	7	−2.033 794 03	$\frac{1}{\sqrt{3}}$H($4p$) − $\frac{1}{\sqrt{2}}$H($4d$) + $\frac{1}{\sqrt{6}}$H($4f$)
	8	−2.033 453 58	He($1s4f\,^1F^o$)
	9	−2.030 818 19	$\frac{1}{\sqrt{3}}$H($4p$) − $\sqrt{\frac{2}{3}}$H($4f$)
	10	−2.030 657 50	He($1s4d\,^1D$)
	11	−2.028 925 58	$\frac{1}{\sqrt{3}}$H($4p$) + $\frac{1}{\sqrt{2}}$H($4d$) + $\frac{1}{\sqrt{6}}$H($4f$)
	12	−2.028 775 73	He($1s4p^1P^o$)

[a] It is understood that H($n\ell$) is accompanied by $He^+(1s)$ and that He($1sn\ell\,^1L$) is accompanied by H^+.

Table 4. $^3\Pi$ states included in the calculations and their dissociation product. In this table, we use the notation H($n\ell$) or He($1sn\ell\,^3L$) to denote the electronic wavefunctions of the corresponding electronic states. Due to the He^+ charge, there is a Stark effect on the hydrogen levels (see the text). The mixing coefficients have been calculated by diagonalizing the perturbation matrix due to the electric field.

	m	Energy (hartree) at $R = 70$ au	Dissociative atomic wavefunctions[a]
$n = 2$	1	−2.132 825 25	He($1s2p\,^1P^o$)
	2	−2.124 918 45	H($2p$)
$n = 3$	3	−2.058 144 10	He($1s3p\,^1P^o$)
	4	−2.056 400 23	$\frac{1}{\sqrt{2}}$H($3p$) + $\frac{1}{\sqrt{2}}$H($3d$)
	5	−2.055 261 05	He($1s3d\,^1D$)
	6	−2.054 565 18	$\frac{1}{\sqrt{2}}$H($3p$) − $\frac{1}{\sqrt{2}}$H($3d$)
$n = 4$	7	−2.033 713 07	He($1s4p^1P^o$)
	8	−2.033 235 84	$\frac{1}{\sqrt{3}}$H($4p$) − $\frac{1}{\sqrt{2}}$H($4d$) + $\frac{1}{\sqrt{6}}$H($4f$)
	9	−2.030 816 42	$\frac{1}{\sqrt{3}}$H($4p$) − $\sqrt{\frac{2}{3}}$H($4f$)

[a] It is understood that H($n\ell$) is accompanied by $He^+(1s)$ and that He($1sn\ell\,^3L$) is accompanied by H^+.

line positions of the ground-state potential of HeH^+. A remarkable agreement has been obtained with the theoretical values of Bishop and Cheung (1979).

The value obtained in this work for the dissociation energy is of 16 464 cm^{-1}. The energy depth in our calculation is therefore less than 9 cm^{-1} too shallow and is to be compared to the result of van Hemert and Peyerimhoff (1990) which is 298 cm^{-1} too large. Following these authors, this discrepancy is indicative of a basis set deficiency. The basis set superposition effect (BSSE) has been evaluated by the counterpoise method and has been found to be negligible.

Table 5. $^1\Delta$ states included in the calculations and their dissociation product. In this table, we use the notation H($n\ell$) or He($1sn\ell\,^1L$) to denote the electronic wavefunctions of the corresponding electronic states. Due to the He^+ charge, there is a Stark effect on the hydrogen levels (see the text). The mixing coefficients have been calculated by diagonalizing the perturbation matrix due to the electric field.

	m	Energy (hartree) at $R = 70$ au	Dissociative atomic wavefunctions[a]
$n = 3$	1	−2.055 406 49	H($3d$)
	2	−2.055 377 12	He($1s3d\,^1D$)
$n = 4$	3	−2.032 068 18	He($1s4f\,^1F^o$)
	4	−2.032 042 21	$\frac{1}{\sqrt{2}}$H($4d$) + $\frac{1}{\sqrt{2}}$H($4f$))

[a] It is understood that H($n\ell$) is accompanied by $He^+(1s)$ and that He($1sn\ell\,^1L$) is accompanied by H^+.

Table 6. $^3\Delta$ states included in the calculations and their dissociation product. In this table, we use the notation H($n\ell$) or He($1sn\ell\,^3L$) to denote the electronic wavefunctions of the corresponding electronic states. Due to the He^+ charge, there is a Stark effect on the hydrogen levels (see the text). The mixing coefficients have been calculated by diagonalizing the perturbation matrix due to the electric field.

	m	Energy (hartree) at $R = 70$ au	Dissociative atomic wavefunctions[a]
$n = 3$	1	−2.055 435 91	He($1s3d\,^1D$) + H^+
	2	−2.055 408 33	$He^+(1s)$ + H($3d$)

[a] It is understood that H($n\ell$) is accompanied by $He^+(1s)$ and that He($1sn\ell\,^3L$) is accompanied by H^+.

In addition, using a B-spline basis set method, we have resolved the vibrational nuclear equation for $^4HeH^+$ and obtained 12 vibrational bound states, as was found in the recent paper of Stanke *et al* (2006).

The $A\,^1\Sigma^+$ and the $a\,^3\Sigma^+$ states have been studied by Kolos (1976) in the adiabatic approximation. They both present weakly attractive potential curves with a minimum at large internuclear distances, $R_e = 5.53$ au and 4.47 au for the singlet and the triplet (respectively), to be compared with our values of 5.53 au and 4.45 au. We have determined the dissociation energies $D_e = 849.71$ cm^{-1} for the A state and $D_e = 379.70$ cm^{-1} for the a state. A study of the vibrational structure of the $a\,^3\Sigma^+$ state of $^4HeH^+$ has been performed by Chibisov *et al* (1996) using the potential energy curve of (Michels 1966) extended by an analytical expression in the asymptotic region. They found that this potential supports five bound vibrational levels, while our resolution of the vibrational motion produced six bound levels. However, the binding energy of the last level is less than 1 cm^{-1}. The largest difference between our energy values and those of Chibisov *et al* is of 2 cm^{-1}. It is also important to note that the non-adiabatic couplings between the $^3\Sigma^+$ states have been neglected in both calculations and could modify significantly the energy of the levels, as it has been shown already for the vibrational structure of the ground state (Stanke *et al* 2006). Finally, in our calculations, we found that four bound vibrational levels are supported by the $A\,^1\Sigma^+$ state of $^4HeH^+$.

Table 7. Active spaces used in state-averaged CASSCF calculations.

n value	$^1\Sigma^+$	$^3\Sigma^+$	$^1\Pi$	$^3\Pi$	$^{1,3}\Delta$
1	$(6\sigma, 2\pi)$ $(X^1\Sigma^+)$ $(9\sigma, 4\pi, 1\delta)$ $(A^1\Sigma^+)$	$(9\sigma, 4\pi, 1\delta)$			
2	$(9\sigma, 4\pi, 1\delta)$	$(9\sigma, 4\pi, 1\delta)$	$(9\sigma, 4\pi, 1\delta)$	$(9\sigma, 4\pi, 1\delta)$	
3	$(12\sigma, 6\pi, 4\delta)$	$(12\sigma, 8\pi, 2\delta)$	$(4\sigma, 8\pi, 6\delta)$	$(4\sigma, 10\pi, 2\delta)$	$(6\sigma, 4\pi, 4\delta)$
4	$(28\sigma, 2\delta)$	(28σ)	$(2\sigma, 13\pi, 2\delta)$		$(6\sigma, 4\pi, 4\delta)$

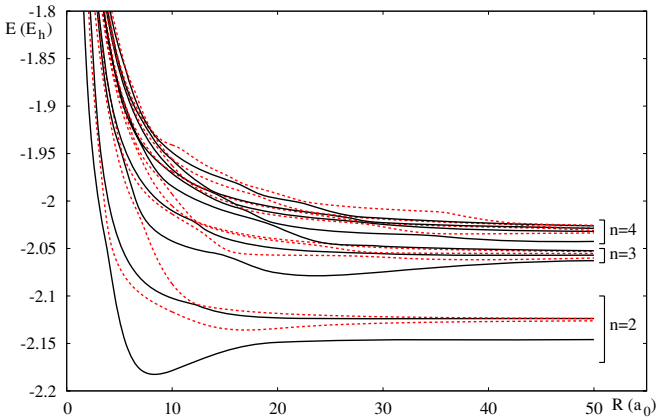

Figure 2. Adiabatic potential energy curves for the $n = 2$–4 $^1\Sigma^+$ states. Solid curves, states dissociating into He($1snl\,^1L$) + H$^+$. Dashed curves, states dissociating into He$^+$($1s$) + H($n\ell$).

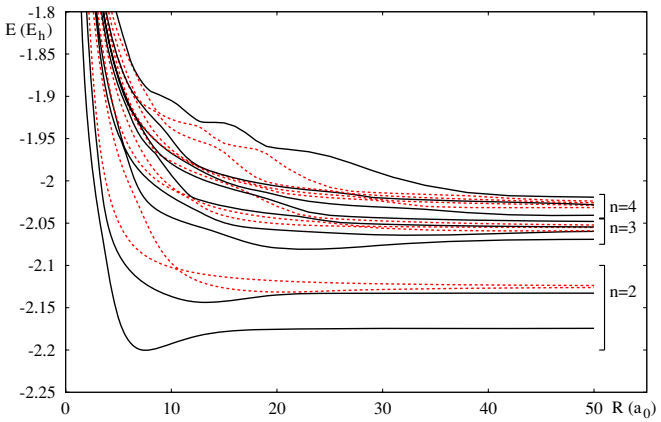

Figure 3. Adiabatic potential energy curves for the $n = 2$–4 $^3\Sigma^+$ states. Solid curves, states dissociating into He($1snl\,^3L$) + H$^+$. Dashed curves, states dissociating into He$^+$($1s$) + H($n\ell$).

3.2. Adiabatic potential energy curves for the first Rydberg $^{1,3}\Sigma^+$ states

The $n = 2$–4 states of HeH$^+$ can be divided into two groups. The first category dissociated asymptotically into H$^+$ and neutral He in an excited $1snl\,^{1,3}L$ state, while the second one dissociated into He$^+$ in its $1s$ ground state and an excited $n\ell$ state of H. Both categories of states alternated along the electronic spectrum resulting in a large number of avoided crossings leading to charge exchange dynamics. For the Σ symmetry, the total number of states up to $n = 4$ is 20 for the singlets and 19 for the triplets. They are shown in figures 2 and 3, respectively. In these figures, the states of the first category are plotted as solid curves while the states of the second category are plotted as dashed curves.

The $n = 2$ manifolds have a very similar behaviour in both singlet and triplet spin symmetries. However, for the singlet states an avoided crossing between the two highest states occurs at an internuclear distance of 50 au. This crossing is understandable once looking at the asymptotical behaviour of those two $^1\Sigma^+$ states, which is governed by the Stark effect. Indeed, at large internuclear distances, the system is composed of a neutral atom, perturbed by an ion. The atomic dissociative states are He($1s2p\,^1P^o$) + H$^+$ and He$^+$($1s$) + H($2s$), respectively for the highest and the lowest state.

If we restrict the description to quadratic effects in the field, the helium state behaves asymptotically in the presence of the H$^+$ charge as

$$E(R) = E^0_{\mathrm{He}(1s2p\,^1P^o)} - \frac{\alpha_{\mathrm{He}(1s2p\,^1P^o)}}{2R^4} \tag{1}$$

and the $2s$ state of H, under the electric field produced by He$^+$, as

$$E(R) = E^0_{\mathrm{He}^+(1s)+\mathrm{H}(2s)} + \frac{3}{R^2} - \frac{\alpha_{\mathrm{H}(2s)}}{2R^4} \tag{2}$$

where E^0 represent the atomic energies. In addition, the $|2s\rangle$ state of hydrogen becomes $\frac{1}{\sqrt{2}}|2s\rangle - \frac{1}{\sqrt{2}}|2p\rangle$.

The first-order Stark effect produces a term proportional to $1/R^2$, which vanishes unless the atomic state is degenerate with a state of opposite parity (Goldman and Cassar 2005). The term proportional to $1/R^4$ is due to the second-order Stark effect, and the constant α is the dipole polarizability. The polarizabilities for the helium states can be found in (Yan 2000, 2002) while the polarizabilities for hydrogen are obtained analytically (Radzig and Smirnov 1985). The result is that while the helium state presents an almost flat asymptotic curve, the hydrogen state decreases to its atomic value, and a crossing occurs in the analytical model at $R = 50$ au, almost exactly as in the *ab initio* calculation.

From figure 4, we see that the asymptotic $n = 2$ states are correctly described using the Stark effect up to order 2. To a lesser extent, it is also the case of the $n = 3$ singlet states (see figure 5): for example, the analytical model reproduces the crossing which occurs at 90 au between the 11th and 12th states dissociating respectively into He$^+$($1s$) + H($3s$) and He($1s3p\,^1P^o$) + H$^+$ (see table 1).

In the Born–Oppenheimer approximation, in which the quantum chemical calculations are performed, these crossings are avoided. However, the large amplitude and the narrowness of the non-adiabatic couplings at those points indicate that a full diagonal diabatic representation at the crossing is perfectly justified.

It is clear from figures 2 and 3 that the number of avoided crossings increases strongly with n and that their positions are shifted to larger internuclear distances. Those avoided

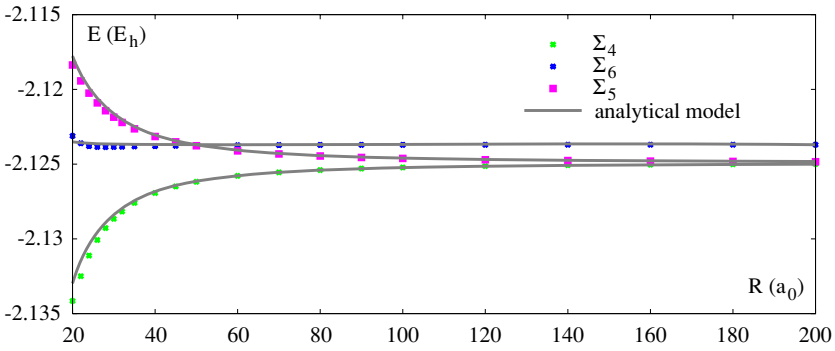

Figure 4. Asymptotic behaviour of the three highest $n = 2\ ^1\Sigma^+$ states. The numbers in the subscript refer to the value of m as defined in table 1.

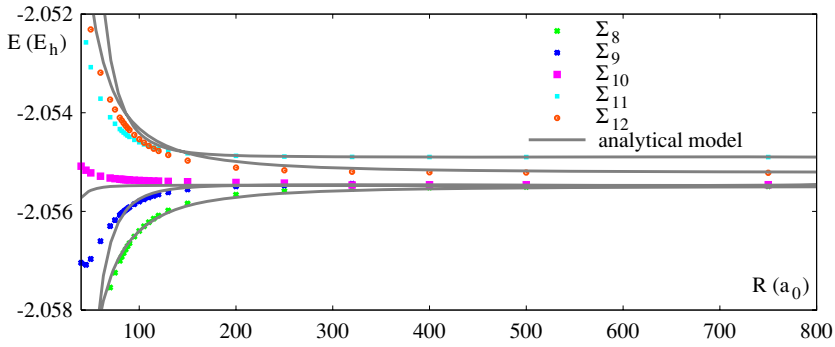

Figure 5. Asymptotic behaviour of the five highest $n = 3\ ^1\Sigma^+$ states.

crossings mask partially the intrinsic oscillatory behaviour of the higher states that has been observed in previous calculations (Boutalib and Gadea 1992). This behaviour has been related to the nodal structure of the Rydberg orbitals which may start to be important in the $n = 4$ manifold and can be clearly seen in the last two $^3\Sigma^+$ states. The second observation is that the states belonging to different manifolds are very close in energy, especially at internuclear distances smaller than 10 au. In addition, well-defined avoided crossings couple the last state of a manifold to the first state of the next manifold at large internuclear distances (7 au between $n = 2$ and $n = 3$ and 18 au between $n = 3$ and $n = 4$ for the singlet symmetry).

Finally, due to the presence of the $n = 5$ states, very close in energy and not adequately described in our calculations, the representation of the highest $n = 4$ states is probably less accurate than for the other members of the Rydberg series.

The comparison can be made with the previous work of Green *et al* (1974a, 1974b, 1976, 1978) for the $n = 2$ singlet and triplet states in the range $R = 1$–5 au and with the data of Klüner *et al* (1999) for the three first singlet states in the range $R = 1$–10 au. The different sets of results are very similar for both spin symmetries, the present calculations being systematically more stable in energy.

We also note that Klüner *et al* (1999) have associated, at short internuclear distances, the last state of the $n = 2$ manifold in their calculations as dissociating into $He(1s2p\ ^1P^o)$ + H^+ while due to the crossing involving this state at 50 au, it actually corresponds to $He^+(1s)$ + H ($n = 2$) (see table 1). This is very important since these authors are interested in the electron transfer mechanism and they have eliminated the last $n = 2$ state from their dynamical calculations.

Table 8. Location of the principal non-adiabatic radial couplings for the $n = 1$–3 Σ^+ states.

$^1\Sigma^+$ states	R (a_0)	$^3\Sigma^+$ states	R (a_0)
3–4	3.9	2–3	3.6
4–5	3.1	3–4	2.9
5–6	12.7	4–5	10.6
6–7	7.0	5–6	3.5, 6.8
7–8	2.9, 5.2	6–7	5.5
8–9	4.1	7–8	4.5
9–10	12.0	8–9	10.8, 12.3, 28.0
9–11	12.2	9–10	3.6, 12.1, 26.0
10–11	4.0, 6.6, 12.2	10–11	5.7, 8.8
11–12	2.7, 5.4, 8.8, 25.0		

Table 9. Location of the principal non-adiabatic radial couplings for the $n = 1$–3 Π states.

$^1\Pi$ states	R (a_0)	$^3\Pi$ states	R (a_0)
3–4	7.5	3–4	7.6
4–5	3.5, 18.8	4–5	4.5, 18.8
5–6	18.1	5–6	18.3

For the $n = 3$ manifold, only Green *et al* provide a full set of results for both singlet and triplet states. The differences with our data are more important than for the $n = 2$ states in both spin multiplicities, especially for the highest states which undergo avoided crossings with the lowest $n = 4$ states.

Tables 8 and 9 give the location of all the major avoided crossing points for singlet and triplet states which have been determined by an analysis of the calculated radial non-adiabatic couplings (see section 4.1).

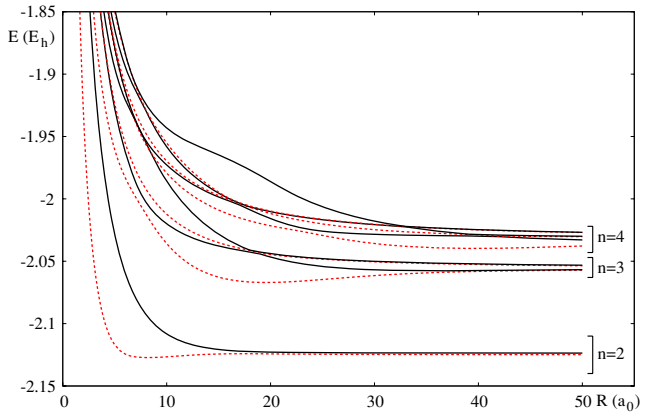

Figure 6. Adiabatic PEC of the $n = 2$–4 $^1\Pi$ states. Solid curves, states dissociating into He($1s n\ell\,^1L$) + H$^+$. Dashed curves, states dissociating into He$^+$($1s$) + H($n\ell$).

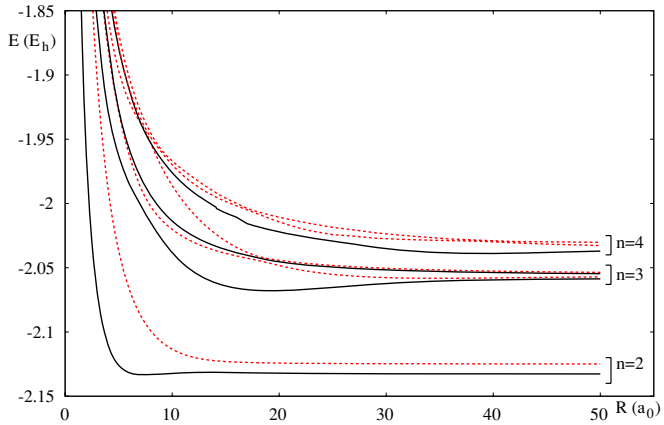

Figure 7. Adiabatic PEC of the $n = 2$–4 $^3\Pi$ states. Solid curves, states dissociating into He($1s n\ell\,^3L$) + H$^+$. Dashed curves, states dissociating into He$^+$($1s$) + H($n\ell$).

3.3. Adiabatic potential energy curves for the first Rydberg $^{1,3}\Pi$ and $^{1,3}\Delta$ states

The potential energy curves of the $^1\Pi$ and $^3\Pi$ states are presented in figures 6 and 7, respectively. The PEC have again a very similar behaviour for both spin multiplicities. Indeed, the first and the third state seem to present a shallow well, and we also see that an avoided crossing between the last three $n = 3$ states occurs at $R = 18$ au. Finally, the last $n = 3$ state and the first $n = 4$ state interact strongly at about 8 au.

Once again, the qualitative comparison with the results of Green *et al* for $n = 2$–3 is good but there are some differences. The avoided crossing mentioned above occurs at $R = 20$ au rather than at $R = 18$ au in our work, and we also see that the energy separation at the avoided crossing between the third and fourth state (internuclear distance of about 8 au) is larger in our calculation.

Finally, the PEC for the Δ states are presented in figure 8. They seem to be almost independent of the spin multiplicity. In the work of Green *et al*, the two $n = 4$ PEC present an avoided crossing, which is not the case in this work.

It should be noted that the calculation of the Δ states is more difficult than for the other symmetries. This is due

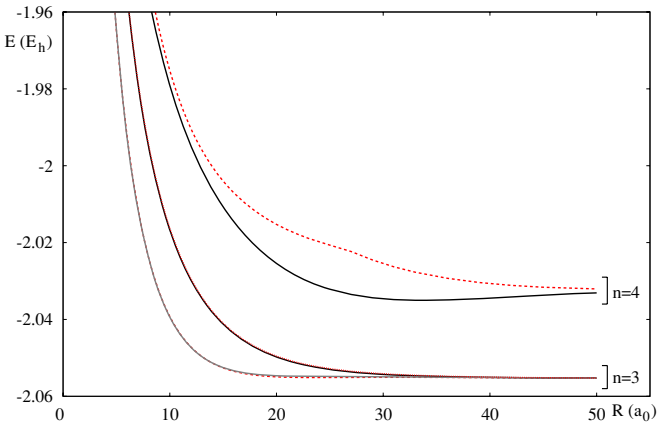

Figure 8. Adiabatic PEC of the $n = 3$–4 $^1\Delta$ and of the $n = 3$ $^3\Delta$ states (full and dashed lines, respectively). Solid black curves, states dissociating into He($1s n\ell\,^{1,3}L$) + H$^+$. Dashed curves, states dissociating into He$^+$($1s$) + H($n\ell$). Grey curve, the $^3\Delta$ state dissociating into He($1s n\ell\,^3L$) + H. Dotted curve, the $^3\Delta$ state dissociating into He$^+$($1s$) + H($n\ell$).

to the fact that MOLPRO can only use Abelian groups, and the C_{2v} subgroup of $C_{\infty v}$ is used for the diatomic molecules. In this group, the Σ^+ and Δ states are calculated within the same CI matrix diagonalization and it is sometimes difficult to separate the states of those symmetries. The same is true for the Φ states, which correspond to the same irreducible representations as the Π states in C_{2v}.

4. Non-adiabatic corrections

We write the total Hamiltonian as the sum of an electronic part, $H^{\rm el}$, and a nuclear kinetic part, $T^{\rm N}$, which itself can be developed into a radial ($H^{\rm rad}$) and a rotational ($H^{\rm rot}$) part:

$$\begin{aligned} H &= T^{\rm N} + H^{\rm el} \\ &= H^{\rm rad} + H^{\rm rot} + H^{\rm el}. \end{aligned}$$

In the electronic Hamiltonian, the mass polarization term has been neglected. Using the electronic wavefunctions $\zeta_{i,\Lambda}$, solutions of the electronic Schrödinger equation

$$H^{\rm el}\zeta_{i,\Lambda}(\mathbf{r};R) = U_i(R)\zeta_{i,\Lambda}(\mathbf{r};R),$$

the total wavefunction is expressed as a product of an electronic and a nuclear wavefunction: $\Psi(\mathbf{R},\mathbf{r}) = \sum_{i,\Lambda}\zeta_{i,\Lambda}(\mathbf{r};R)\psi_{i,\Lambda}(\mathbf{R})$, where $\mathbf{r}$ and $\mathbf{R}$ stand for the electron and nuclear coordinates, respectively. Λ is the quantum number associated with L_z, the projection of the electronic orbital angular momentum $\mathbf{L}$ onto the z axis.

As the nuclear Hamiltonian is separable, the nuclear wavefunction is given by the product $\psi_i(\mathbf{R}) = \psi_i(R)\,|K\Lambda\rangle$, where $|K\Lambda\rangle$ is an eigenfunction of the operators $\mathbf{K}^2$ and K_z, and $\mathbf{K}$ being the total angular momentum.

Using this development, the Schrödinger equation can be expressed as

$$\sum_{j,\Lambda'}\langle\zeta_{i,\Lambda}|H^{\rm rad} + H^{\rm rot}|\zeta_{j,\Lambda'}\rangle\psi_{j,\Lambda'} + (U_i - E)\psi_{i,\Lambda} = 0\,,$$

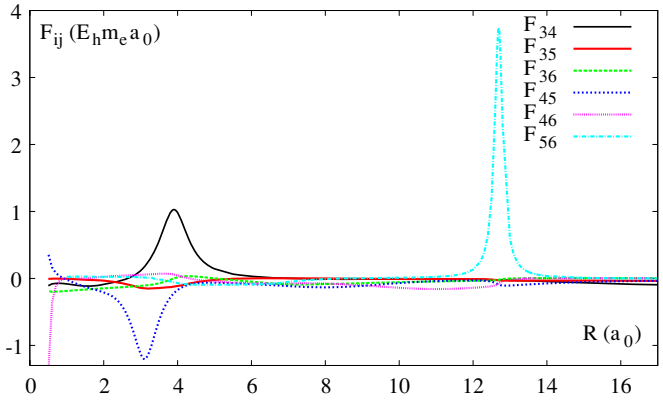

Figure 9. Radial non-adiabatic coupling matrix elements between the $n = 2\,^1\Sigma^+$ states. The numbers in the subscript refer to the value of m as defined in table 1.

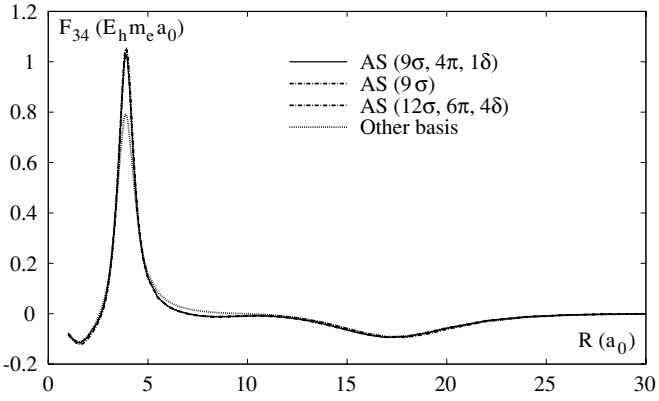

Figure 10. Radial non-adiabatic coupling F_{34} calculated with different active spaces (AS), as well as with the basis from (van Hemert and Peyerimhoff 1990).

where

$$H^{\text{rad}} = -\frac{1}{2\mu}\partial_R^2$$

and

$$H^{\text{rot}} = \frac{1}{2\mu R^2}\mathbf{N}^2 = \frac{1}{2\mu R^2}[\mathbf{K}^2 + \mathbf{L}^2 - 2K_zL_z - K_+L_- - K_-L_+] \quad (3)$$

where $\mathbf{N}$ is the nuclear angular momentum.

4.1. Radial couplings

Using the orthonormality of the electronic wavefunctions, the matrix elements of the radial Hamiltonian are given by

$$\langle\zeta_{i,\Lambda}| - \frac{1}{2\mu}\partial_R^2|\zeta_{j,\Lambda'}\rangle = -\frac{1}{2\mu}\left[\partial_R^2\delta_{ji} + 2\langle\zeta_{i,\Lambda}|\partial_R|\zeta_{j,\Lambda'}\rangle\partial_R + \langle\zeta_{i,\Lambda}|\partial_R^2|\zeta_{j,\Lambda'}\rangle\right]\delta_{\Lambda'\Lambda} = -\frac{1}{2\mu}\left[\partial_R^2\delta_{ji} + 2F_{i\Lambda,j\Lambda'}\partial_R + G_{i\Lambda,j\Lambda'}\right]\delta_{\Lambda'\Lambda}.$$

Since it can be shown that in matrix form $\mathbb{G} = \mathbb{F}^2 + \partial_R\mathbb{F}$ (Baer 2006), we only need to calculate the elements of $\mathbb{F}$, which is block diagonal in Λ. These couplings were calculated using a three-point central difference method implemented in the DDR programme of MOLPRO with a displacement parameter $dR = 0.01$ au.

For the analysis of the radial couplings, we will focus on the $n = 2$ states since all the $k(k-1)/2$ couplings (where k is the number of states for a given Λ) cannot be shown here. We note that the dominant couplings are systematically those connecting two adjacent states (i.e. the couplings $F_{i,i\pm1}$), as shown in figure 9 for the $n = 2$ states. This implies that states of different values of n can interact at the exception of the two $n = 1$ states which are isolated in energy. The dominant couplings are narrow and their maxima correspond to the positions of the avoided crossings given in table 8 for the Σ states and in table 9 for the Π states. The PEC will cross at those points upon diabatization. These couplings are known as 'Landau–Zener couplings' (Zener 1932). The radial couplings presented in figure 9 are of this type. On other hand, some couplings are wider and do not correspond to clear avoided crossings; instead, the PEC are parallel in the coupling region. These couplings arise mainly at large internuclear distances. The dynamics around these couplings is described by the Rosen–Zener theory (Rosen and Zener 1932). Both types of couplings will give rise to very different dynamical behaviours. As an example, we will consider the case of the coupling F_{34} (shown in figure 10), which can be separated in a Landau–Zener coupling (centred around $R \sim 4$ au) and a Rosen–Zener coupling, centred at $R \sim 17$ au. The position and the shape of the long-range coupling are invariant under changes in the level of electron correlation or in the atomic basis set used in the calculation, as illustrated in figure 10.

We observed that some of the radial couplings tend asymptotically to a constant which differs from zero. This behaviour is expected for the couplings between two molecular states of the same symmetry degenerated at infinity when the calculations of the couplings are done using an origin of the electronic coordinates at the centre of the nuclear mass (Belyaev *et al* 2001).

As the final goal of this work is the study of non-adiabatic dynamics involving those couplings, we should note here that a number of authors demonstrated the importance of electron translation factors at high and intermediate energies and proposed different methods to take them into account (Thorson and Delos 1978, Errea *et al* 1994). It was also established that these factors are linked to the choice of the origin of the electronic coordinates (Bransden and McDowell 1992). As we noted the quasi-invariance of the radial couplings under a translation of the origin of the electronic coordinates along the internuclear axis (see figure 11), it appears that the inclusion of translation factors in dynamical simulations will not be necessary.

4.2. Rotational couplings

From equation (3), we can obtain the matrix elements of the rotational Hamiltonian between the electronic and rotational

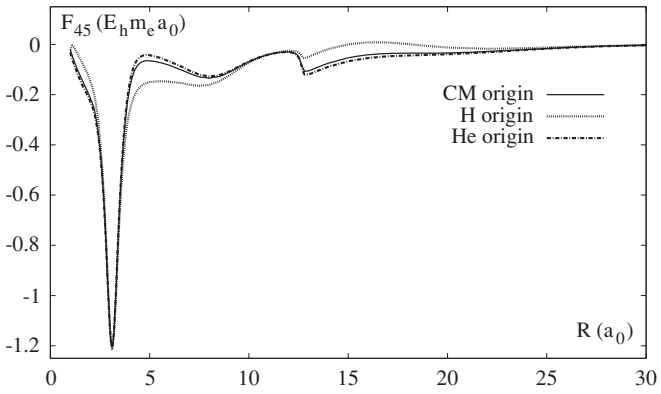

Figure 11. Radial non-adiabatic coupling F_{45} calculated using an origin of the coordinates at the centre of mass, on H or on He.

nuclear functions. They are given by

$$H_{i\Lambda K,j\Lambda' K'} = \langle K\Lambda|\langle\zeta_{i,\Lambda}|H^{\rm rot}|\zeta_{j,\Lambda'}\rangle|K'\Lambda'\rangle$$
$$= \frac{1}{2\mu R^2}\Big\{\big[(K(K+1)-\Lambda^2)\delta_{ij} + \langle\zeta_{i,\Lambda}|L_x^2+L_y^2|\zeta_{j,\Lambda'}\rangle\big]\delta_{\Lambda\Lambda'}$$
$$+2[K(K+1)-\Lambda(\Lambda-1)]^{1/2}\langle\zeta_{i,\Lambda}|{\rm i}L_y|\zeta_{j,\Lambda'}\rangle\delta_{\Lambda',\Lambda+1}$$
$$-2[K(K+1)-\Lambda(\Lambda+1)]^{1/2}\langle\zeta_{i,\Lambda}|{\rm i}L_y|\zeta_{j,\Lambda'}\rangle\delta_{\Lambda',\Lambda-1}\Big\}\delta_{KK'}. \quad (4)$$

We see from the formula above that $L_x^2 + L_y^2$ is an interaction between states of the same Λ value. In particular, the diagonal part $\left(L_x^2 + L_y^2\right)_{ii}$ modifies the energies of the states. This contribution can be evaluated using MOLPRO at the CASSCF level, but we will not report it here since it was shown by Bishop and Cheung (1979) that for the ground state it is of the same order of magnitude as the effect of the mass polarization term, which we have neglected. The same conclusion was reached by Bunker (1968) for H_2. We only mention the fact that asymptotically, these matrix elements behave as R^2, so the corrections to the energies are constants (see equation (4)) when the internuclear distance is large.

The operator iL_y, on the other hand, connects states with $\Delta\Lambda = \pm 1$ and cannot be neglected. Note that the calculation of the matrix elements of iL_y necessitates the simultaneous determination of electronic states of different values of Λ in the same calculation.

The rotational couplings between the $n = 2\ ^1\Pi$ and $^1\Sigma^+$ states are presented in figure 12. Asymptotically, the couplings between states that dissociate into the same atomic species and into the same n manifold are constant. Some rotational couplings between states dissociating into different n manifolds make an exception and behave asymptotically as R, as indicated by Belyaev *et al* (2001). All the couplings between states dissociating into different atomic species tend to zero at large internuclear distances.

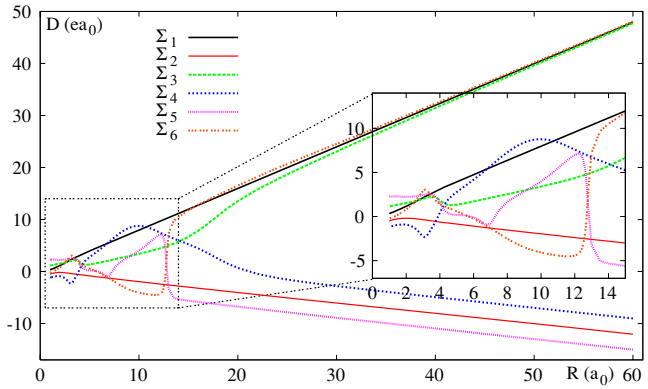

Figure 13. Permanent dipole moments for the $n = 1, 2\ ^1\Sigma^+$ states.

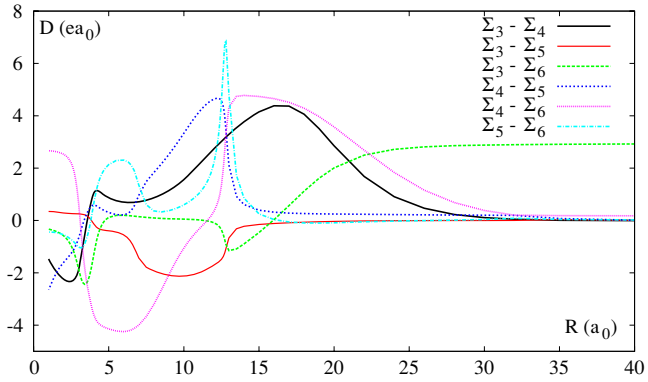

Figure 14. Transition dipole moments between the $n = 2\ ^1\Sigma^+$ states.

5. Adiabatic dipole moments

There are $k(k+1)/2$ (where k is the number of states) dipole matrix elements and we will again restrict our discussion to the $^1\Sigma^+$ states. The permanent adiabatic dipole moments of the $n = 1, 2$ states are represented in figure 13, while the transition dipole moments of the $n = 2$ states are represented in figure 14.

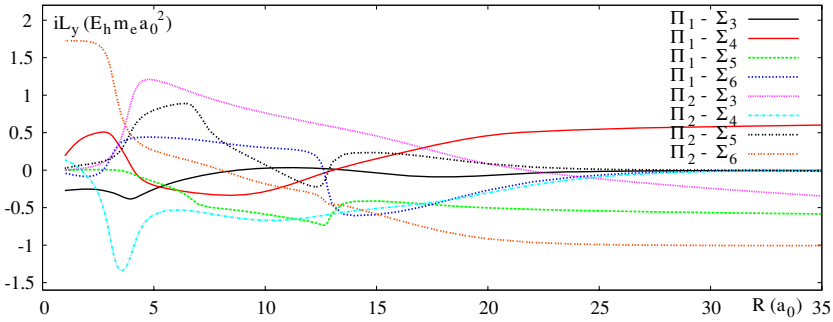

Figure 12. Adiabatic rotational couplings between the $n = 2\ ^1\Sigma^+$ and $^1\Pi$ states. The numbers in the subscript refer to the value of m as defined in table 1.

In a given Λ subspace, the dipole interaction occurs only through the z component. As there is no ambiguity, we will thus write the dipole moment between two states i and j as μ_{ij} instead of $\mu_{z,ij}$.

The behaviour of the dipole moments is consistent with the calculation of the radial couplings, illustrating the relation between the two operators (Macías and Riera 1978) which allows the use of the dipole moment rather than the radial couplings to find a diabatic representation. For example, the crossing between the dipoles μ_{55} and μ_{66} at $R = 12.75$ au corresponds to the sharp radial coupling seen in figure 9 at the same internuclear distance, and is reflected on the transition dipole moment between the two states, μ_{56}, which presents a sharp peak in the crossing region. Conversely, when two permanent dipoles have a peak of opposite value, as do μ_{44} and μ_{55} at $R = 3.1$ au, the sign of the transition dipole μ_{45} changes abruptly. Again, this is linked to an avoided crossing between the fourth and fifth states at the same internuclear distance.

As can be seen from figure 13, all the permanent dipole moments μ_{ii} behave asymptotically as R, since the origin of the coordinates is at the nuclear centre of mass and not on one of the atoms. As the reduced mass of ^{4}HeH$^+$ is $\mu = 0.805$ amu, the helium and the hydrogen nuclei are situated approximatively at $-0.2R$ and $0.8R$ of the origin, respectively. The permanent dipole moment can then be divided into a nuclear and an electronic part. The nuclear contribution is of $0.4R$ and is identical for all states, while the electronic contribution is of $0.4R$ for the He($1sn\ell\,^1L$) + H$^+$ states and of $-0.6R$ for the He$^+$($1s$) + H($n\ell$) states. For the latter, there is an additional contribution from the interaction between the helium $1s$ electron and the hydrogen $n\ell$ electron which explains that the permanent dipole moments for these states do not tend to the same asymptotic value.

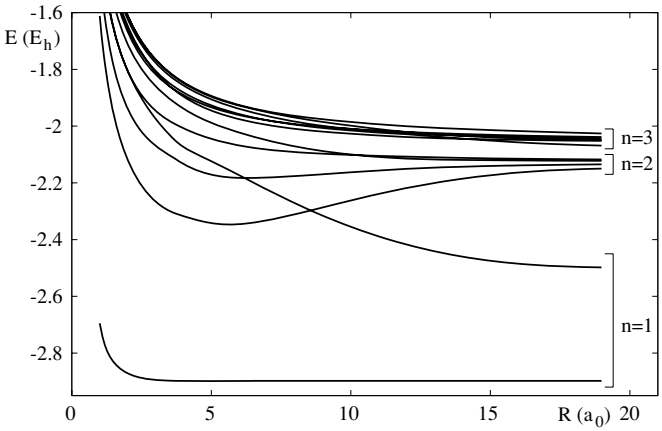

Figure 15. Diabatic PEC of the $n = 1$–$3\ ^1\Sigma^+$ states.

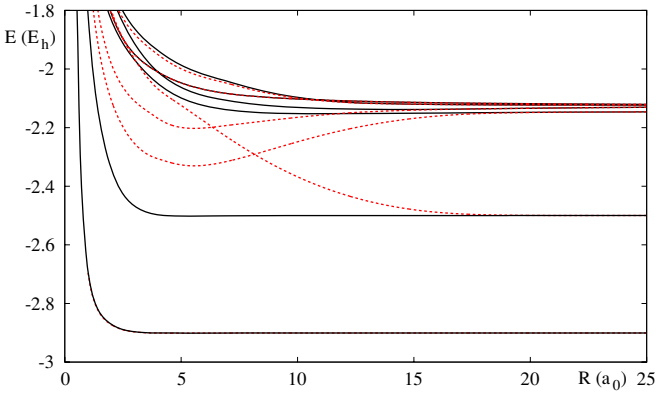

Figure 16. Comparison of the diabatic PEC of the $n = 1$ and $n = 2\ ^1\Sigma^+$ states diabatized independently (solid curves) or as a whole (dashed curves).

6. Diabatic representation of the Rydberg states

The diabatic representation is defined so as to cancel the $\mathbb{F}$ matrix, which is the case if the adiabatic-to-diabatic transformation matrix $\mathbb{D}$ satisfies the matrix equation

$$\partial_R \mathbb{D} + \mathbb{F} \cdot \mathbb{D} = 0. \tag{5}$$

The diabatic potential energy curves are then given as the diagonal elements of the transformed matrix $\mathbb{U}^d = \mathbb{D}^{-1} \cdot \mathbb{U} \cdot \mathbb{D}$. We solve equation (5) by continuity using a grid of 2000 points, starting from $R = 60$ au where we require that the adiabatic and diabatic representations are identical (so that $\mathbb{D} = \mathbb{I}$). It should also be noted that, as we calculate the non-adiabatic radial coupling at the CASSCF level, we also use the CASSCF energies, which differ slightly from the CI energies presented in section 3.

In our diabatization procedure, we will not consider the complete $\mathbb{F}$ matrix, keeping only the couplings $F_{i,i+1}$ and putting all the other couplings to zero. This approximation, which amounts to a succession of two-states cases, is used for various reasons. The first one is that, as was shown in section 4.1, those couplings are systematically the most important ones. Secondly, it has been shown by Zhu and Nakamura (1997) that this approximation gives correct results in dynamical calculations even for low energies, which is confirmed by our calculations of the electron-transfer cross sections in the $n = 2$ manifold (Loreau *et al* 2010). Thirdly, some of the couplings which we neglect remain non-zero at large internuclear distance. This phenomenon is known and has been discussed in detail by Belyaev *et al* (2001), but raises a problem in our diabatization method. Indeed, our procedure is based on the fact that the adiabatic and diabatic representations coincide at $R = \infty$, which is not the case if the couplings do not vanish. As a consequence, these residual couplings, although small, influence the diabatic PEC at large R, a feature which is of course undesirable.

We will consider the $^1\Sigma^+$ states as an example of the diabatization procedure. The result of the diabatization for these states up to $n = 3$ is given as an example in figure 15.

It is clear that the diabatization alters considerably the shape of the ground state. From figure 16, we see that this is essentially due to the coupling F_{12} since the same behaviour is observed when the $n = 1$ states are diabatized independently.

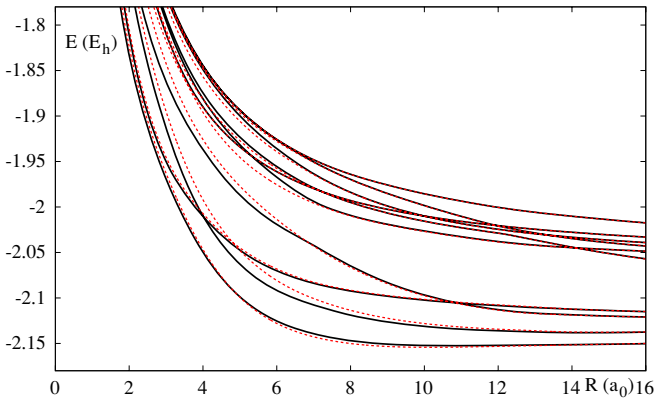

Figure 17. Comparison of the diabatic PEC of the $n = 2$ and $n = 3$ $^1\Sigma^+$ states diabatized independently (solid curves) or as a whole (dashed curves).

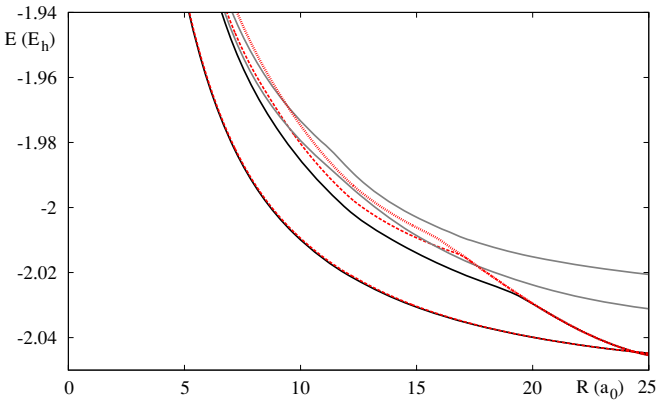

Figure 18. Effect of the $n = 4$ states on the last two $n = 3$ states. Solid black curves, the fifth and sixth $n = 3$ diabatic states. Dashed curves, the same states, but diabatized with the first $n = 4$ state. The fifth $n = 3$ state is left unaltered, but the avoided crossing of the sixth $n = 3$ state is shifted from $R = 20$ au to $R = 17$ au. Dots, the sixth $n = 3$ state diabatized with the first and second $n = 4$ state (solid grey curves). The avoided crossing is further shifted to $R = 16$ au.

The first excited state also changes dramatically, crossing the entire $n = 2$ manifold in the diabatic representation, which is due to the coupling F_{23} (see figure 16). However, one must remember that the non-adiabatic coupling between the two first $^1\Sigma^+$ states is of the Rosen–Zener type, and that therefore the diabatic representation of those states has little physical significance. Likewise, the influence of the two first $^1\Sigma^+$ states on the diabatic representation of the $n = 2$ states is very important but has little effect on the non-adiabatic dynamics in the $n = 2$ manifold, as has been observed in the calculation of charge exchange cross section between He^+ and H at low energies (Loreau *et al* 2010). To our knowledge, the only other work on the diabatic representation of the PEC of the HeH^+ ion has been done by Klüner *et al* (1999) using the quasi-diabatization procedure proposed by Pacher *et al* (1988). These authors compare a 3-state (the three lowest $n = 2$ states) and a 4-state (adding the second $n = 1$ state) diabatization in a small interval of internuclear distances (0.8 au $\leqslant R \leqslant$ 5.4 au). It is concluded that the inclusion of the $n = 1$ state does not modify the diabatic PEC of the $n = 2$ manifold, and this state is therefore neglected in wavepacket simulations of charge exchange processes involving $n = 2$ states. Although we arrive at the same conclusion regarding the dynamics, our method gives significantly different diagonal as well as non-diagonal matrix elements of the electronic Hamiltonian in the diabatic representation.

On the other hand, the effect of the interaction between the $n = 2$ and $n = 3$ manifolds through the F_{67} matrix element is relatively small, as shown in figure 17.

Finally, the description of the diabatic $n = 3$ states necessitates to take some higher-lying states into account, since the highest diabatic state undergoes an avoided crossing around $R = 20$ (as can be seen in figure 2) with the first $n = 4$ state. The inclusion of the first two $n = 4$ states in the diabatization, while leaving the first five $n = 3$ states unaltered, clearly influences the sixth state by shifting the position of the avoided crossing to smaller values of R, as illustrated in figure 18. Therefore, a more correct description of the last $n = 3$ diabatic state should include more $n = 4$ states, even though we are only considering the couplings between adjacent states.

7. Conclusions

We present an accurate description of 66 low-lying adiabatic states of HeH^+. Using the MOLPRO package and a large adapted basis set, the potential energy curves of the $n = 1$–3 as well as most of the $n = 4$ states of the molecular ion have been obtained and compared to previous theoretical works. The radial and rotational non-adiabatic coupling matrix elements, as well as the dipole matrix elements, have been calculated for all the $n = 1$–3 states. The radial couplings allow us to switch to the diabatic representation which is used to treat dynamical processes involving the ion. This material has been used to calculate the cross section of the photodissociation of the ion (Sodoga *et al* 2009) and the cross sections for the charge transfer processes $He^+(1s) + H(n\ell) \longrightarrow He(1sn'\ell'^{\,1,3}L) + H^+$ at low energy (Loreau *et al* 2010).

Acknowledgments

We thank M Godefroid for helpful discussions. This work was supported by the Fonds National de la Recherche Scientifique (IISN projects) and by the Action de Recherche Concertée ATMOS de la Communauté Française de Belgique. PP and PQ are respectively research associate and senior research associate of the Belgian FRS–FNRS. J Loreau thanks the FRIA for financial support.

Appendix. Basis set

Tables A1, A2 and A3 list additional basis sets for hydrogen and for the singlet and triplet states of helium.

Table A1. Additional basis functions for hydrogen.

	Coefficient	Exponent		Coefficient	Exponent
2*s*	0.000 144	19.907 407	3*p*	0.024 590	0.986 107
	−0.005 010	8.988 620		0.260 387	0.181 062
	−0.059 868	0.645 915		0.903 505	0.051 409
	−0.123 387	0.071 221		−1.874 014	0.007 783
	0.891 720	0.024 689		−0.287 389	0.003 281
3*s*	0.017 083	1.000 840	4*p*	0.015 689	1.015 267
	0.120 859	0.272 819		0.170 182	0.186 800
	0.381 641	0.093 336		0.625 077	0.053 622
	0.782 727	0.023 846		−2.040 089	0.009 383
	−2.036 422	0.019 287		2.535 609	0.002 477
	1.594 513	0.004 250			
			3*d*	0.050 502	0.199 534
4*s*	0.013 653	11.939 994		0.495 617	0.051 732
	0.167 164	1.060 859		1.609 201	0.018 241
	0.662 095	0.188 361		1.213 582	0.007 264
	−3.032 473	0.029 081			
	4.828 012	0.007 375	4*d*	0.077 845	0.083 401
	−4.362 099	0.001 197		0.454 482	0.021 517
				−0.894 944	0.003 285
2*p*	0.005 698	3.101 143			
	0.067 894	0.567 270	4*f*	0.026 401	0.033 813
	0.407 521	0.158 596		0.169 866	0.010 591
	1.082 414	0.052 537		0.204 085	0.004 109
	0.800 233	0.020 01			

Table A2. Additional basis functions for the singlet states of helium.

	Coefficient	Exponent		Coefficient	Exponent
2*s*	0.002 760	99.181 545	3*p*	0.002 929	4.673 075
	0.030 509	10.536 516		0.037 026	0.848 515
	0.196 191	1.905 592		0.244 477	0.227 656
	0.775 469	0.424 822		0.806 379	0.070 757
	−3.722 470	0.029 920		−2.050 784	0.007 911
3*s*	−0.001 952	99.838 262	4*p*	0.002 547	4.629 236
	0.012 286	49.068 205		0.076 795	0.396 874
	0.151 694	2.653 277		0.488 599	0.081 760
	0.516 699	0.309 173		3.304 293	0.017 020
	−3.156 883	0.038 398		−4.848 362	0.013 667
	4.383 564	0.006 064		2.305 369	0.002 285
4*s*	−0.004 235	99.861 298	3*d*	0.062 634	0.102 716
	0.011 613	49.188 130		0.430 990	0.026 362
	0.316 811	0.732 304		0.551 594	0.008 950
	−2.495 917	0.035 479			
	4.534 324	0.009 221	4*d*	0.077 839	0.082 347
	4.267 928	0.001 472		0.454 447	0.021 503
				−0.894 818	0.003 283
2*p*	0.000 152	19.984 152			
	0.002 135	4.719 990	4*f*	0.026 447	0.033 780
	0.025 319	1.021 806		0.170 021	0.010 582
	0.160 069	0.292 204		0.204 038	0.004 106
	0.592 704	0.101 345			
	1.066 547	0.039 590			
	0.527 114	0.016 351			

Table A3. Additional basis functions for the triplet states of helium.

	Coefficient	Exponent		Coefficient	Exponent
2*s*	0.006 837	99.181 525	3*p*	0.002 497	4.675 067
	0.067 529	10.551 100		0.035 791	0.789 129
	0.269 982	2.355 836		0.247 261	0.205 234
	0.759 139	0.643 556		0.833 266	0.065 732
	−3.666 553	0.037 246		−2.061 784	0.007 542
3*s*	−0.000 849	99.836 273	4*p*	0.013 260	1.567 909
	0.012 336	49.044 874		0.137 119	0.284 565
	0.156 413	3.473 103		0.208 845	0.076 404
	0.448 487	0.589 924		3.155 372	0.015 570
	−3.036 160	0.043 579		−4.866 015	0.013 266
	4.329 233	0.006 971		2.376 480	0.002 506
4*s*	−0.004 869	99.860 674	3*d*	0.016 008	0.199 406
	0.015 055	49.185 022		0.156 978	0.051 714
	0.327 369	1.070 000		0.508 950	0.018 239
	−2.490 977	0.042 209		0.383 308	0.007 266
	4.623 855	0.011 100			
	−4.295 313	0.001 760	4*d*	0.010 397	0.218 719
				0.112 909	0.056 369
2*p*	0.005 913	4.650 435		0.423 743	0.019 585
	0.158 917	0.458 934		−0.906 780	0.003 352
	0.939 676	0.102 736			
	1.256 290	0.030 224	4*f*	0.018 968	0.038 973
				0.139 803	0.012 212
				0.230 793	0.004 712
				0.999 016	0.000 133

References

Badnell N R 1986 *J. Phys. B: At. Mol. Phys.* **19** 3827

Badnell N R 1997 *J. Phys. B: At. Mol. Opt. Phys.* **30** 1

Baer M 2006 *Beyond Born–Oppenheimer* (New York: Wiley) p 9

Belyaev A K, Egorova D, Grosser J and Menzel T 2001 *Phys. Rev.* A **64** 052701

Bishop D M and Cheung L M 1979 *J. Mol. Spectrosc.* **75** 462

Boutalib A and Gadea F X 1992 *J. Chem. Phys.* **97** 1144

Bransden B H and McDowell M R 1992 *Charge Exchange and the Theory of Ion–Atom Collisions* (Oxford: Clarendon)

Bunker P R 1968 *J. Mol. Spectrosc.* **28** 422

Chibisov M I, Yousif F B, Van der Donk P J T and Mitchell J B A 1996 *Phys. Rev.* A **54** 5997

Coxon J A and Hajigeorgiou G 1999 *J. Mol. Spectrosc.* **193** 306

Dumitriu I and Saenz A 2009 *J. Phys. B: At. Mol. Opt. Phys.* **42** 165101

Dunning T H 1989 *J. Chem. Phys.* **90** 1007

Eissner W, Jones M and Nussbaumer H 1974 *Comput. Phys. Commun.* **8** 270

Engel E A, Doss N, Harris G J and Tennyson J 2005 *Mon. Not. R. Astron. Soc.* **357** 471

Errea L F, Harel C, Jouin H, Méndez L, Pons B and Riera A 1994 *J. Phys. B: At. Mol. Opt. Phys.* **27** 3603

Frebel A *et al* 2005 *Nature* **434** 871

Giesbertz K J H, Baerends E J and Gritsenko O V 2008 *Phys. Rev. Lett.* **101** 033004

Goldman and Cassar 2005 Atoms in strong fields *Handbook of Atomic, Molecular and Optical Physics* ed Drake (Berlin: Springer)

Green T A, Browne J C, Michels H H and Madsen M M 1974a *J. Chem. Phys.* **61** 5186

Green T A, Browne J C, Michels H H and Madsen M M 1974b *J. Chem. Phys.* **61** 5198

Green T A, Michels H H and Browne J C 1976 *J. Chem. Phys.* **64** 3951

Green T A, Michels H H and Browne J C 1978 *J. Chem. Phys.* **69** 101
Harris G J, Lyans-Gray A E, Miller S and Tennyson J 2004 *Astrophys. J.* **617** L143
Hogness T R and Lunn E C 1925 *Phys. Rev.* **26** 44
Jurek M, Spirko V and Kraemer W P 1995 *Chem. Phys.* **193** 287
Klüner T, Thiel S and Staemmler V 1999 *J. Phys. B: At. Mol. Opt. Phys.* **32** 4931
Knowles P J and Werner H-J 1985 *Chem. Phys. Lett.* **15** 259
Kolos W 1976 *Int. J. Quantum Chem.* **X** 217
Kolos W and Peek J M 1976 *Chem. Phys.* **12** 381
Loreau J, Desouter-Lecomte M, Sodoga K, Lauvergnat D and Vaeck N 2010 in preparation
Macías A and Riera A 1978 *J. Phys. B: At. Mol. Phys.* **11** L489
Michels H H 1966 *J. Chem. Phys.* **44** 3834
Moorhead J M, Lowe R P, Maillard J-P, Wehlau W H and Bernath P F 1988 *Astrophys. J.* **326** 899
Pacher T, Cederbaum L S and Köppel H 1988 *J. Chem. Phys.* **89** 7367
Pedersen H B *et al* 2007 *Phys. Rev. Lett.* **98** 223202
Radzig A A and Smirnov B M 1985 *Reference Data on Atoms, Molecules and Ion* (Berlin: Springer)
Richings G W and Karadakov P B 2007 *Mol. Phys.* **105** 2363
Roberge W and Dalgarno A 1982 *Astrophys. J.* **255** 489
Rosen N and Zener C 1932 *Phys. Rev.* **40** 502
Rosmej F B, Stamm E and Lisitsa V S 2006 *Europhys. Lett.* **73** 342
Sodoga K, Loreau J, Lauvergnat D, Justum Y, Vaeck N and Desouter-Lecomte M 2009 *Phys. Rev.* A **80** 033417
Stanke M, Kedziera D, Bubin S and Adamowicz L 2008 *Phys. Rev.* A **77** 022506
Stanke M, Kedziera D, Molski M, Bubin S, Barysz M and Adamowicz L 2006 *Phys. Rev. Lett.* **96** 233002
Thorson W R and Delos J B 1978 *Phys. Rev.* A **18** 117
van Hemert M C and Peyerimhoff S D 1990 *J. Chem. Phys.* **94** 4369
Werner H-J and Knowles P J 1985 *J. Chem. Phys.* **82** 5053
Werner H-J *et al* 2006 MOLPRO, version 2006.1 A package of *ab initio* programs, see http://www.molpro.net
Woon D E and Dunning T H 1994 *J. Chem. Phys.* **100** 2975
Yan Z C 2000 *Phys. Rev.* A **62** 052502
Yan Z C 2002 *J. Phys. B: At. Mol. Opt. Phys.* **35** 2713
Zener C 1932 *Proc. R. Soc.* **137** 696
Zhu C and Nakamura H 1997 *J. Chem. Phys.* **106** 2599